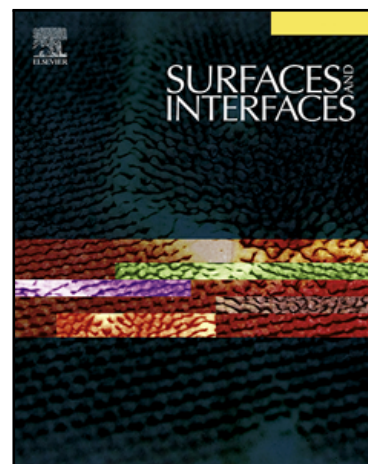


Journal Pre-proof

Highly efficient and stable PANI/TRGO nanocomposites as active materials for electrochemical detection of dopamine

Daria Minta , Zoraida González , Sonia Melendi-Espina , Grażyna Gryglewicz

PII: S2468-0230(21)00678-7
DOI: <https://doi.org/10.1016/j.surfin.2021.101606>
Reference: SURFIN 101606



To appear in: *Surfaces and Interfaces*

Received date: 8 September 2021
Revised date: 8 November 2021
Accepted date: 14 November 2021

Please cite this article as: Daria Minta , Zoraida González , Sonia Melendi-Espina , Grażyna Gryglewicz , Highly efficient and stable PANI/TRGO nanocomposites as active materials for electrochemical detection of dopamine, *Surfaces and Interfaces* (2021), doi: <https://doi.org/10.1016/j.surfin.2021.101606>

This is a PDF file of an article that has undergone enhancements after acceptance, such as the addition of a cover page and metadata, and formatting for readability, but it is not yet the definitive version of record. This version will undergo additional copyediting, typesetting and review before it is published in its final form, but we are providing this version to give early visibility of the article. Please note that, during the production process, errors may be discovered which could affect the content, and all legal disclaimers that apply to the journal pertain.

© 2021 Published by Elsevier B.V.

Highly efficient and stable PANI/TRGO nanocomposites as active materials for electrochemical detection of dopamine

Daria Minta^a, Zoraida González^{b*}, Sonia Melendi-Espina^c, Grażyna Gryglewicz^a

^a Department of Process Engineering and Technology of Polymer and Carbon Materials, Faculty of Chemistry, Wrocław University of Science and Technology, Gdańska 7/9, 50-344 Wrocław, Poland

^b Instituto de Ciencia y Tecnología del Carbono, INCAR-CSIC, Francisco Pintado Fe 26, 33011 Oviedo, Spain;

^c School of Engineering, University of East Anglia, Norwich Research Park, Norwich NR4 7TJ, United Kingdom

*Corresponding author: zoraidag@incarcsic.es

ABSTRACT:

Thermally reduced graphene oxides (TRGOs), produced at 400 and 700 °C, and polyaniline (PANI) were used for one-pot facile hydrothermal synthesis of binary nanocomposites (PANI/TRGO). The morphology and chemical composition of these materials were thoroughly characterized by means of scanning electron microscopy, nitrogen sorption at 77 K, elemental analysis, X-ray photoelectron spectroscopy, X-ray diffraction, and sheet resistance measurements. Cyclic voltammetry, differential pulse voltammetry and electrochemical impedance spectroscopy were used for electrochemical characterization. The scanning electron microscopy (SEM) observation revealed that the morphology of TRGOs has a crucial impact on the distribution of PANI in the composites. A more homogenous distribution of PANI was achieved for PANI/TRGO-700 due to the higher degree of exfoliation of the starting material TRGO-700. The synthesized composites were investigated as modifiers of glassy carbon electrodes (GCEs) for the electrochemical sensing of dopamine. Both, the PANI distribution and an appropriate oxygen content are key for DA sensing. Thus, the better performance of PANI/TRGO-700 as an active material was revealed, achieving a LOD of 430 nM, an excellent sensitivity ($6.7 \mu\text{A } \mu\text{M}^{-1}$) and stability after 30 days.

KEYWORDS: hydrothermal treatment, composites, graphene materials, conducting polymers, electrochemical sensor, dopamine

1. Introduction

Dopamine (DA) is one of the most crucial neurotransmitters in the human brain [1]. Among other neurotransmitters, DA is highly responsible for regulating the pleasure and reward pathways [2]. An inadequate release of DA can initiate mental health issues, while its high production can lead to addiction and, as a result, to long-term dejection [2]. Very low DA levels can be indicators of Parkinson's and Alzheimer's diseases [3]. Therefore, the monitoring of DA levels provides very important information about a patient's health. In this context, different sensing technologies are being widely investigated for greater simplicity and improved sensitivity of DA sensing approaches [4]. Among them, high-performance liquid chromatography [5], optical sensors [3], fluorescence spectrometry [6] are being developed, along with the very promising electrochemical sensors [3,7]. The simplicity, fast response and low-cost of electrochemical sensing has recently attracted considerable research interest in this field [8].

Currently, research concerning electrochemical sensors is mainly focused on the development of new and facile-synthesized materials able to improve the working parameters of sensors and facilitate real-time detection [3]. On this basis, it is also essential to consider that DA coexists with several interfering species, such as uric acid (UA), ascorbic acid (AA), glucose or epinephrine, which have similar oxidation potentials [9]. To overcome selectivity problems for the target analyte, it is beneficial to design materials that can specifically catalyze its redox processes, for example, decreasing its oxidation potential [10]. In this regard, graphene materials, conductive polymers, and their composites are being increasingly studied [3,10–13]. Graphene-like materials with heteroatoms, such as oxygen, and defects in their structure, present a limited electrical conductivity [14,15]. However, it has been previously demonstrated that negative oxygen moieties have a beneficial impact on DA detection, attracting its cationic form to the electrode/electrolyte

interface [16]. To apply graphenes as active electrode materials for DA electrochemical detection, it is crucial to select the most appropriate synthesis procedure, to be able to tune the oxygen content. A simple approach is the thermal exfoliation/reduction of graphite oxide (GrO), which enables the controlled tailoring of the oxygen content [17,18]. Moreover, to combine good electrochemical properties and improved interactions between the surface of active materials and analyte, PANI/graphene material composites have been developed [10]. PANI has been increasingly studied in the field of electrochemical sensing due to its low cost and simple synthesis, good electrical conductivity, and environmental stability [19,20]. Furthermore, the long polymer chains and π -rich structure of PANI can facilitate the immobilization of DA molecules via the interaction between the DA phenyl ring and polymer [12].

Numerous articles have shown the successful application of reduced graphene oxides (rGOs), PANI and their composites with inorganic materials such as metals, metal oxides and metal nanoparticles for the detection of different analytes [21–23]. However, there are still a few works presenting the performance of binary PANI/rGO composites for the electrochemical detection of DA. Yang et al. [24] obtained electrochemically rGO, which exhibits good performance for DA detection, with a LOD of 500 nM at neutral pH. Gao et al. [25] synthesized GO by a modified Hummers method and used the resultant material to modify a GCE for DA detection (LOD=270 nM at pH 5.0). A simple exfoliation of graphite oxide and subsequent reduction by hydrazine and ammonia was used by Kim et al. [26] to prepare a graphene material as a GCE modifier. In the electrochemical detection of DA, the platform showed a LOD of 2.64 μ M over a wide linear range of 4–100 μ M. Related to conductive polymers, a tetragonal star-like polyaniline microstructure synthesized under hydrothermal conditions (120 °C/6 h) was applied by Jin et al. for DA detection, achieving a LOD of 700 nM [27]. Furthermore, Manivel et al. [19] used PANI-GO fibrous

nanocomposites for the simultaneous determination of DA, UA and AA. The composite was synthesized by in situ chemical oxidative polymerization of the aniline monomer in a GO suspension. DA detection was possible in the range from 2 to 18 μM with a LOD of 500 nM and a sensitivity for DA of 2 $\mu\text{A } \mu\text{M}^{-1}$. Yang et al. [28] applied AuNP@polyaniline core-shell nanocomposites for simultaneous DA and AA detection. The obtained LOD values were 5 and 8 μM , respectively.

In this work, PANI/TRGO-based electrochemical sensors were evaluated for their ability to selectively detect dopamine. To the best of our knowledge, this is the first study in which these graphene materials, prepared through the thermal exfoliation/reduction of GrO, were used as components of nanocomposites with PANI and subsequently tested as active electrode materials for DA detection. The two TRGOs obtained at different temperatures (400 and 700 $^{\circ}\text{C}$) were treated with PANI under hydrothermal conditions. The resultant composites differed in their morphology and elemental composition, leading to different behaviors during DA sensing. The appropriate oxygen content and homogenous distribution of PANI in the PANI/TRGO-700 composite was responsible for its remarkable electrochemical performance, reaching a LOD of 430 nM and a sensitivity of 6.71 $\mu\text{A } \mu\text{M}^{-1}$.

2. Experimental

2.1 Synthesis of the starting materials

GrO was obtained by the oxidative treatment of anthracene oil (AO)-derived graphite using a modified Hummers method [29]. GrO was then exfoliated by flash pyrolysis in a tubular furnace at a controlled temperature (below 300 $^{\circ}\text{C}$) and then ramp-heated (5 $^{\circ}\text{C } \text{min}^{-1}$) up to the final temperature (400 and 700 $^{\circ}\text{C}$, $t_{\text{R}}=1$ h) under inert atmosphere (N_2 flow: 200 $\text{mL } \text{min}^{-1}$) [17]. The as-prepared thermally reduced graphene oxides were labelled as TRGO-400 and TRGO-700.

PANI was synthesized using a common oxidative polymerization procedure that was previously reported [30]. Briefly, 500 mg of aniline monomer (Sigma Aldrich, Poznan, Poland) and 5 mg of Triton X-100 were added to a solution composed of 20 mL of Milli-Q water and 10 mL of 1 M HCl. The solution was then ultrasonicated for 30 min at 0–5 °C. Then, the mixture was stirred, and ammonium persulfate (APS) was added at a 1:2 molar ratio of aniline:APS. The polymerization was performed at 0–5 °C for 6 h. The final product was filtered and washed with Milli-Q water and methanol until the supernatant reached neutral pH. Finally, the product was vacuum dried at 60 °C for 12 h.

2.2 Hydrothermal synthesis of the composite materials (PANI/TRGO)

PANI/TRGO composites were prepared using a simple one-step hydrothermal treatment. First, 50 mg of the corresponding TRGO were dispersed in Milli-Q water and ultrasonicated for 30 min. Afterwards, 50 mg of PANI were added to the solution and ultrasonicated. The dispersion was placed into an autoclave (Parr Instrument Company, Moline, IL, USA), and the reaction was performed at 180 °C for 8 h with constant stirring (200 rpm). The autogenic pressure was ~8.8 bar. After the reaction, the product was washed with Milli-Q water and finally vacuum dried overnight at 60 °C. The resulting composite materials were labelled PANI/TRGO-400 and PANI/TRGO-700.

2.3 Preparation of the working electrodes

Firstly, glassy carbon electrodes (GCEs) were polished using alumina oxide and washed with Milli-Q water. Then, the cleaned electrodes were modified with 2.5 µL of a suspension prepared by mixing (with 3 h of ultrasonication) 4 mg of the starting graphene material or corresponding PANI/TRGO composite, and 1 mL of dimethylformamide (DMF, Sigma Aldrich, Saint Louis,

USA)/Milli-Q water solution (v/v ratio 1:1). After that, the electrodes were dried in a furnace at 60 °C for 10 min before being used.

2.4 Characterization of the materials

The morphology of the starting materials (TRGOs, PANI) and subsequent composites (PANI/TRGO) was examined by means of scanning electron microscopy (SEM, using a FEI model Quanta FEG 650 instrument operating at 25 kV, Hillsboro, Oregon, USA). The crystalline structure was determined using X-ray diffraction (XRD, Bruker D8 Advance diffractometer, operating at 40 kV and 40 mA, Karlsruhe, Germany). The specific surface area was determined by applying the BET equation to the nitrogen adsorption isotherms obtained at 77 K on an Autosorb IQ gas sorption analyser (Quantachrome, Boynton Beach, FL, USA). The total C, H, N and O contents of the samples were determined with LECO-CHNS-932 and LECO-VTF-900 microanalysers (Geleen, The Netherlands), respectively. The chemical surface composition was determined by means of X-ray photoelectron spectroscopy (XPS) analysis using a VG-Microtech Multilab 3000 spectrometer (SPECS, Germany) equipped with a hemispherical electron analyser and a MgK α ($h\nu = 1253.6$ eV) X-ray source. The type of carbon bonding and the oxygen and nitrogen functional groups in the samples were estimated by curve fitting the C1s and N1s spectra using a Gaussian-Lorentzian peak shape after performing a Shirley background correction. The XPS spectra were calibrated with respect to the C1s signal at a binding energy of 284.5 eV. In addition, a Jandel RM3000+ test unit attached to a Jandel cylindrical four-point probe head (Jandel Engineering, Leighton Buzzard, UK) was used to evaluate the sheet resistance of the studied samples [31,32]. For these measurements, films of ~ 1 cm² of the starting and composite materials were deposited onto glass slides. These films were made by depositing on the substrate a sufficient

volume of the corresponding suspensions previously described and drying them at 80 °C until solvent evaporated. An average of 4 measurements per film was taken.

2.5 Electrochemical measurements

The electrochemical characterization of the synthesized materials (both the starting and composite materials) was performed in a laboratory-made three-electrode cell with a modified GCE, Ag/AgCl/3.5 M KCl (i.e., 0.205 V vs. NHE) and a graphite rod as the working, reference, and counter electrodes, respectively. Cyclic voltammetry (CV) measurements were carried out at potentials ranging from -0.5 to 0.8 V at increasing scan rates (v_{scan} , from 2 to 250 mV s⁻¹), using 0.1 M phosphate-buffered saline solution (PBS) containing 100 μM DA as the electrolyte (pH value as indicated). Electrochemical impedance spectroscopy (EIS) experiments were performed at frequencies from 0.1 to 10⁵ kHz using a DC potential of 0.27 V. The selected electrolyte consisted of PBS (pH = 7.0) and 10 mM [Fe(CN)₆]^{3-/4-}, as a redox probe to obtain preliminary information about the electron transfer resistance of the different materials. Furthermore, the calibration curves of DA were obtained by differential pulse voltammetry (DPV) tests with optimized parameters, including the holding time at starting potential (20 s), pulse amplitude (225 mV), pulse width (195 ms), pulse period (200 ms) and pulse increase (5 mV). All experiments were carried out at room temperature with a VMP3 potentiostat-galvanostat (Bio-Logic, France).

3. Results and discussion

3.1 Characterization of the starting and composite materials

The morphologies of the starting materials (PANI, TRGO-400 and TRGO-700) and their composites (PANI/TRGO-400 and PANI/TRGO-700) were investigated by means of SEM (Figure 1).

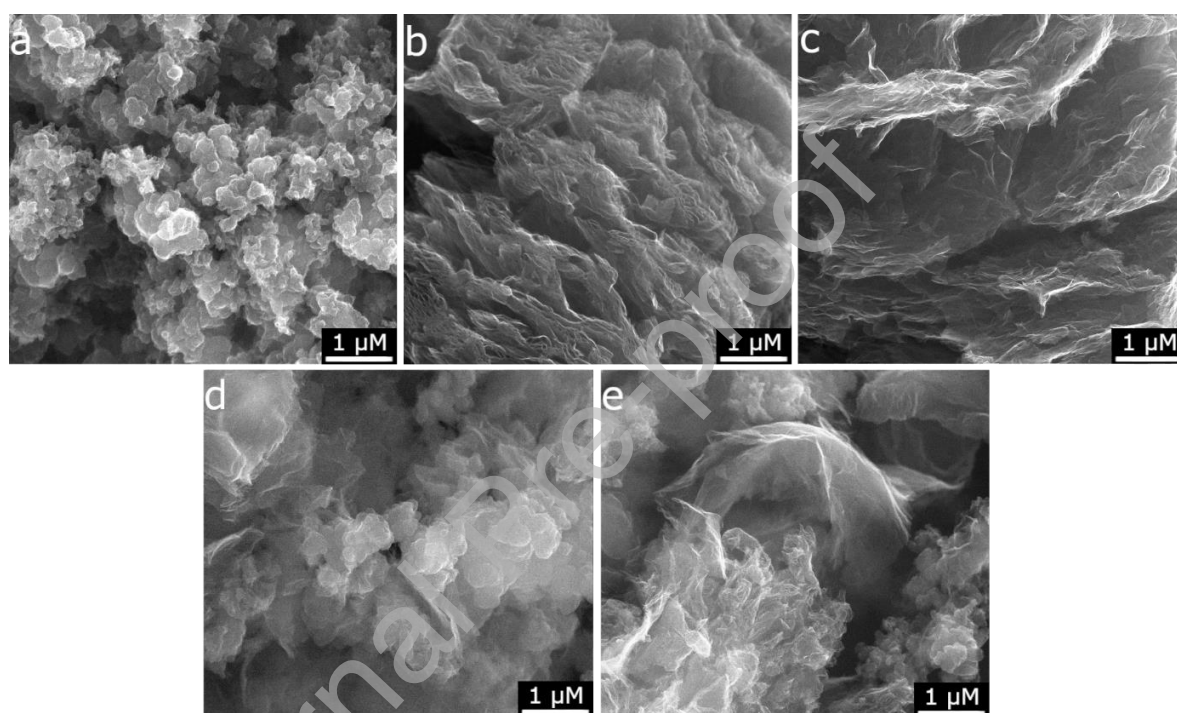


Figure 1. SEM images of (a) PANI, (b) TRGO-400, (c) TRGO-700, (d) PANI/TRGO-400 and (e) PANI/TRGO-700.

As previously reported, PANI mainly consists of coral-shaped and agglomerated nanoparticles (Figure 1a) [33]. Regarding the graphene materials, both TRGOs are composed of typical corrugated layers, resulting from the thermal exfoliation and reduction steps (Figure 1b and 1c) [18,34]. However, compared to TRGO-700, TRGO-400 does not seem to be fully exfoliated, as some accordion-type structures [35] are distinguishable. After hydrothermal treatment of the PANI and TRGO mixture, the resultant composites exhibit significantly different morphologies

depending on the TRGO used as starting material. For PANI/TRGO-400, the presence of aggregated PANI particles covering the surface of the graphene sheets is more evident. According to Figure 1, the exfoliation degree of TRGO-400 is lower than that of TRGO-700; therefore, the homogenous distribution of the PANI chains between the graphene flakes is harder despite the high pressure applied during hydrothermal treatment (~8.8 bar). In contrast, a more efficient incorporation of PANI between the graphene sheets can be observed in the case of TRGO-700 due to its higher exfoliation degree. Moreover, the autogenic pressure can promote the introduction of PANI between the graphene layers. This implies a homogeneous distribution of PANI nanoparticles in the PANI/TRGO-700 composite. The above finding is supported by XRD results (Figure S1, Supporting Information). A diffraction peak at $23.9 - 25.6^\circ$ (JCPDS card no. 72-0634), corresponding to periodicity parallel to the polymer chains of PANI, is observed for both composites. This peak overlaps with the one assigned to the (002) plane of the rGO structure [36,37]. A less intense diffraction peak at 2θ of 43.6° corresponds to the (100) plane of rGO structure [30]. The peak recorded in the range of $10.1 - 13.2$ is referred to PANI [38]. The calculated average interlayer distance (d_{002}) for TRGO-400 is higher than that of its composite (0.3651 vs. 0.3641 nm), which is in agreement with the distribution of PANI chains mainly on the surface of graphene layers, thus causing their compression. In contrast, when examining PANI/TRGO-700, the interlayer distance increases (0.3465 vs. 0.3497 nm), which can be explained by the higher separation of the graphene nanosheets as a result of the incorporation of PANI between them. As expected, the PANI/TRGO composites have a significantly lower BET surface area than the TRGOs, due to the PANI contribution (Table 1). An over threefold decrease in the S_{BET} value has been observed due to the very low surface area of PANI. Lowering the specific surface area of composites could be beneficial for their electrochemical application as

sensing materials due to a marked decrease in capacitive currents [16]. Regarding the chemical composition of the studied materials, Table 1 shows the results obtained by elemental analysis (wt. % in bulk) and XPS analysis (at. %) of the composites and their starting components. The distributions of the oxygen and nitrogen functional groups are summarized in Table 2.

Table 1. Characteristics of the starting and composite materials.

Sample	EA (wt. %)				XPS (at. %)		S_{BET} (m^2g^{-1})	Sheet resistance (Ωsq^{-1})
	C	H	O	N	O	N		
PANI	65.0	3.9	21.4	9.7	9.6	8.2	35	6.22×10^7
TRGO-400	80.8	1.0	18.0	0.2	10.1	-	494	3.20×10^6
TRGO-700	90.3	1.5	8.1	0.1	5.1	-	523	2.37×10^4
PANI/TRGO-400	74.3	2.6	17.5	5.6	8.7	3.5	131	1.86×10^6
PANI/TRGO-700	80.0	2.7	11.7	5.6	6.1	2.5	143	9.84×10^4

Considering the starting TRGOs and according to previously reported results, TRGO-700 has a lower oxygen content than TRGO-400 (8.1 vs. 18.0 wt. %, Table 1) and consequently a higher Csp^2 content (66.5 vs. 55.2 at. %, Table 2), resulting from the higher reduction degree achieved by applying a higher temperature during thermal treatment [18]. The incorporation of PANI chains into the graphene materials leads to composites with a remarkable increase in the total nitrogen content, reaching 5.6 wt. % for both composites (Table 1). However, the surface nitrogen concentration of PANI/TRGO-400, as determined by XPS, is significantly higher than that of PANI/TRGO-700 (3.5 vs. 2.5 at. %, Table 1). This finding also corroborates that PANI/TRGO-700 has a more significant incorporation of polymer chains between the graphene layers than PANI/TRGO-400, where PANI is mostly located on the surface of the graphene sheets (see Figure 1). Following the results obtained from the elemental and XPS analyses (Table 1), the oxygen content in PANI/TRGO-700 is significantly lower than PANI/TRGO-400 (11.7 vs. 17.5 wt. %, 6.1 vs. 8.7 at. %), which is related to the higher degree of reduction of TRGO-700. Figure 2 shows the

deconvoluted C1s and N1s high-resolution core-level XPS spectra of the composite materials. The XPS spectra of PANI and the TRGOs are available in the Supporting Information (Figure S2). The C1s core level spectra of the composites were deconvoluted into five components, which are attributed to graphitic sp^2 -carbon (C=C, 284.5 eV), C-N bonding (C-N, 285.6 eV), hydroxyl and epoxy groups (C-O, 286.5 eV), carbonyl (C=O, 287.6 eV) and carboxylic groups (COOH, 289.0 eV) [39].

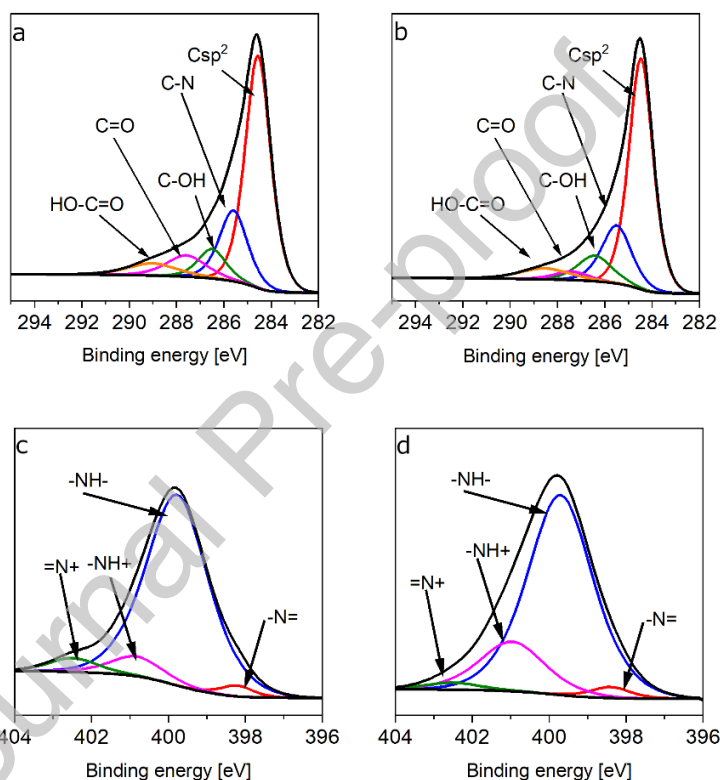


Figure 2. Deconvolution of the (a, b) C1s core-level XPS spectra of PANI/TRGO-400 and PANI/TRGO-700, respectively, and (c, d) N1s core-level XPS spectra of PANI/TRGO-400 and PANI/TRGO-700, respectively.

As follows from the XPS results, hydrothermal treatment of the TRGOs in the presence of PANI leads to a significant decrease in the Csp^2 content and, consequently, to more $Csp^3/C-N$ in the

composites. This is the result of the incorporation of conductive polymer into the composite materials. In any case, the C_{sp^2} content in PANI/TRGO-700 is still higher than that in PANI/TRGO-400 (56.4 vs. 50.9 at. %, Table 2). Additionally, PANI/TRGO-700 has slightly higher amounts of both hydroxylic and carboxylic functional groups, which can have a positive impact on its electrochemical performance for DA detection [16]. The N1s core level spectra of the composites were deconvoluted into four components corresponding to imine ($-N=$, 398.2 eV), amine ($-NH-$, 399.5 eV), positively charged amine-derived nitrogen species ($-NH^+$, 400.8 eV) and protonated imine ($-N^+$, 402.5 eV) [39]. Moreover, according to the literature, the degree of protonation is highly related to the electrical conductivity of a material [40]. The degree of protonation is higher for PANI/TRGO-700 (20.0 vs. 11.4%), which may positively contribute to its behavior as a sensing platform for DA [41].

The above mentioned results are in agreement with the sheet resistance measurements carried out on the films obtained from both the starting and composite materials. According to the data summarized in Table 1, TRGO-700 shows a lower value than TRGO-400 (2.37×10^4 vs $3.20 \times 10^6 \Omega \text{ sq}^{-1}$) as a result of the better restoration of the C_{sp^2} network at the higher temperature. PANI/TRGO-700 presents a higher sheet resistance value than the starting material TRGO-700, which is due to the incorporation of PANI. However, this composite exhibits a lower resistance than PANI/TRGO-400 (9.84×10^4 vs. $1.86 \times 10^6 \Omega \text{ sq}^{-1}$, Table 1), thus indicating that this composite is a more suitable active electrode material for DA detection.

Table 2. Results of C1s and N1s spectra deconvolution (at. %)

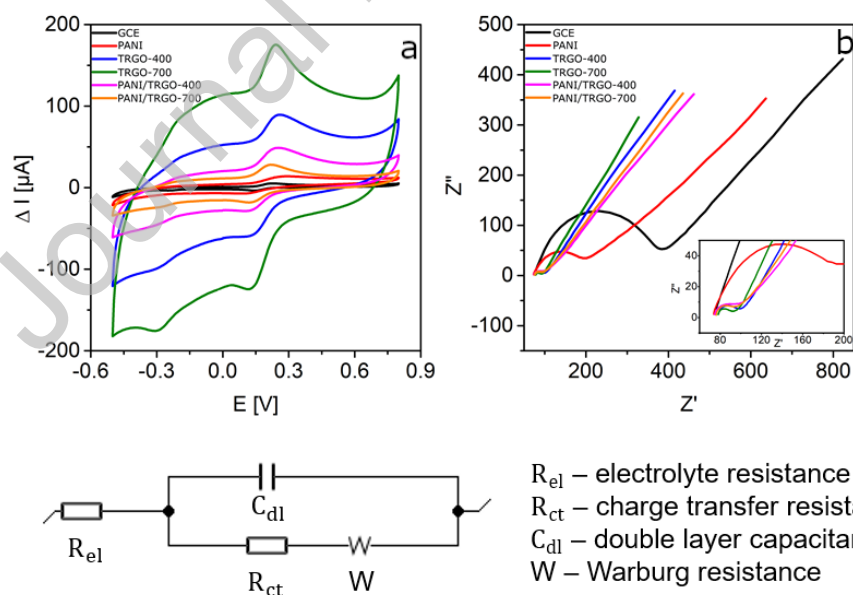
SAMPLE	C1s peak deconvolution					N1s peak deconvolution				P _s %
	C _{sp} ²	C _{sp} ³ /C-N	C-OH	C=O	O=C-OH	-N=	-NH-	-NH ⁺	=N ⁺	
PANI	43.1	21.2	7.0	4.7	4.2	0.2	5.8	1.8	0.2	25.0
TRGO-400	55.2	7.4	12.6	3.4	11.3	-	-	-	-	-
TRGO-700	66.5	9.1	7.6	4.3	7.4	-	-	-	-	-
PANI/TRGO-400	50.9	17.1	7.1	7.4	5.3	0.1	3.0	0.3	0.1	11.4
PANI/TRGO-700	56.4	17.5	8.9	3.0	5.6	0.1	1.9	0.5	-	20.0

P_s – degree of protonation calculated as the ratio of protonated nitrogen groups to the total nitrogen content.

3.2 Electrochemical behavior of the PANI/TRGO composite materials for DA detection

3.2.1. Preliminary characterization of the PANI/TRGO composites

Cyclic voltammetry (CV) experiments were carried out to obtain preliminary information about the electrochemical performance of composites and their starting components for DA detection. Figure 3a shows cyclic voltammograms (CVs) recorded on bare and modified GCEs in PBS solution (pH 7.0) containing 100 μM DA at a scan rate of 100 mV s⁻¹.



R_{el} – electrolyte resistance
 R_{ct} – charge transfer resistance
 C_{dl} – double layer capacitance
 W – Warburg resistance

Figure 3. CVs recorded on the bare and modified GCEs in a 0.1 M PBS (pH 7.0) solution containing 100.0 μM DA at a scan rate of 100 mV s^{-1} (a). Nyquist plots recorded on the bare and modified GCEs in PBS (pH=7.0) solution containing 10 mM $[\text{Fe}(\text{CN})_6]^{3-/4-}$ at a formal potential of 0.27 V and a frequency range of 0.1–10⁵ kHz (b). The inset shows an expanded view of the high-frequency region of the Nyquist plots. The selected equivalent circuit is shown below the plots to fit the impedance data.

The bare GCE and GCE after modification with PANI displayed negligible electrochemical responses for DA redox processes [2]. However, when using TRGOs as active electrode materials, the performance of both electrodes significantly improve, showing well-developed anodic and cathodic peaks related to the dopamine/o-dopaminoquinone and leucodopaminochrome/dopaminochrome redox pairs, respectively [41]. Even though significant DA oxidation currents of 31.3 and 58.5 μA are measured (Figure S3) on the GCEs modified with TRGO-400 and TRGO-700, respectively, there is also a significant contribution in capacitive currents, which is related to the developed surface area of both graphene materials (SBET $\sim 500 \text{ m}^2 \text{ g}^{-1}$, Table 1). According to our previous results, the capacitive current contribution can negatively impact on the electrochemical performance of sensors [16,20]. In this context, the modification of a GCE with the composite materials shows markedly enhanced electrochemical behavior. On both composite-based electrodes, the capacitive currents significantly decrease, in agreement with their lower specific surface areas (131 and 143 $\text{m}^2 \text{ g}^{-1}$ for PANI/TRGO-400 and PANI/TRGO-700, respectively). Furthermore, anodic peaks related to DA oxidation are well developed for both composite materials (oxidation currents of 21.9 and 13.4 μA for PANI/TRGO-400 and PANI/TRGO-700, respectively); however, there is a lower overpotential in the case of PANI/TRGO-700 (217.4 vs. 245.3 mV).

EIS measurements were carried out to gain insight into the electron transfer behavior of the modified GCEs during testing. Figure 3b shows the Nyquist plots recorded on the different electrodes using $[\text{Fe}(\text{CN})_6]^{3-/4-}$ as the redox probe. Moreover, the equivalent circuit selected to fit the impedance data summarized in Table 3 is also shown. According to reported studies, the diameter of the semicircle developed in the high frequency range is proportional to the charge transfer resistance (R_{ct}) of the electrode [42]. On the bare GCE, a well-shaped semicircle was developed, corresponding to a very high R_{ct} value of 270 Ω . After modification with PANI, the radius significantly decreases according to the conductive properties of the polymer. However, the decrease is more pronounced after modifying the GCE with TRGOs and PANI/TRGOs (Table 3), indicating the lower charge transfer resistance of these electrodes. As expected, the values calculated for the composite materials are slightly higher than those corresponding to the starting TRGOs due to the incorporation of PANI in the graphene materials. PANI/TRGO-700 exhibits a lower R_{ct} value than PANI/TRGO-400, confirming the previous CV data and the calculated degree of protonation (Table 2).

Table 3. Impedance data measured for the bare and modified GCE electrodes

Electrode material	R_{ct} (Ω)
GCE	270.1
PANI	113.6
TRGO-400	15.78
TRGO-700	10.61
PANI/TRGO-400	21.35
PANI/TRGO-700	17.56

3.2.2. Determination of the optimum pH values and kinetics of the DA anodic process on composite-based electrodes

With the aim of obtaining better electrochemical performance of composite-based sensors for DA detection, the pH of the supporting PBS solution is a key parameter to be optimized [43]. The influence of solution pH on DA oxidation was investigated using CV measurements at pH values ranging from 5.8 to 8.0 (Figure 4a and b). Figure S4 shows the baseline corrected CVs that were used to measure the DA oxidation currents. Furthermore, the impact of pH on both the anodic peak potentials and their associated currents was demonstrated (Figure 4c–d).

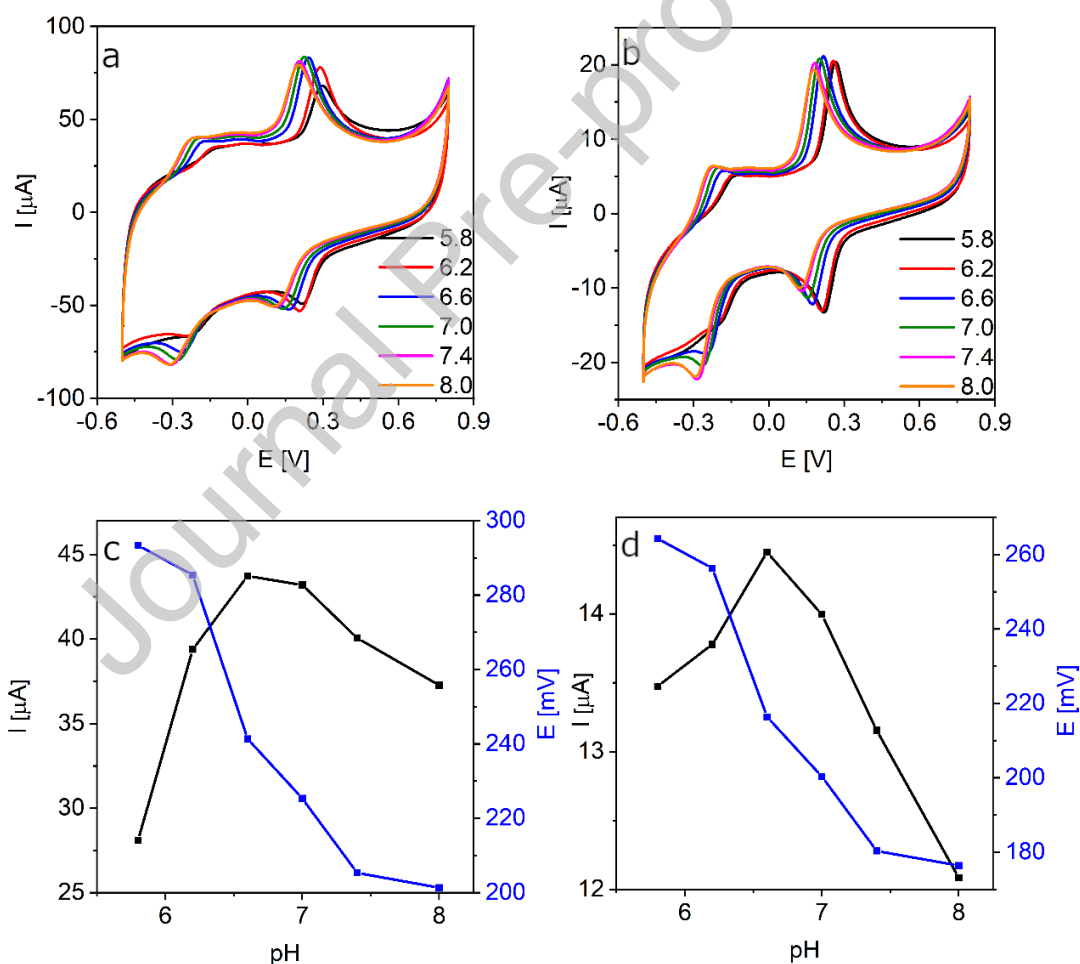


Figure 4. CVs recorded ($v_{\text{scan}} = 100 \text{ mV s}^{-1}$) at increasing pH values on GCEs modified with the composites (a) PANI/TRGO-400 and (b) PANI/TRGO-700 in 0.1 M PBS solution containing 100 μM of DA. Influence of the selected pH on the oxidation current and peak potential values on GCEs modified with (c) PANI/TRGO-400 and (d) PANI/TRGO-700.

Both PANI/TRGO-400 and PANI/TRGO-700 exhibit an optimized pH of 7.0 (very close to the physiological pH). This value was selected in the search for a compromise between the overpotentials and anodic currents measured when evaluating DA oxidation on the two composites. It is important to note that PANI/TRGO-700, showing a lower oxidation peak potential value (200.4 vs. 225.3 mV for PANI/TRGO-400) which is related to its lower oxygen content, also displays a lower anodic current corresponding to DA oxidation (14.0 vs. 43.2 μA for PANI/TRGO-400). However, as previously stated, the lower capacitive currents recorded on PANI/TRGO-700 can have a positive influence on its subsequent electrochemical performance for DA sensing.

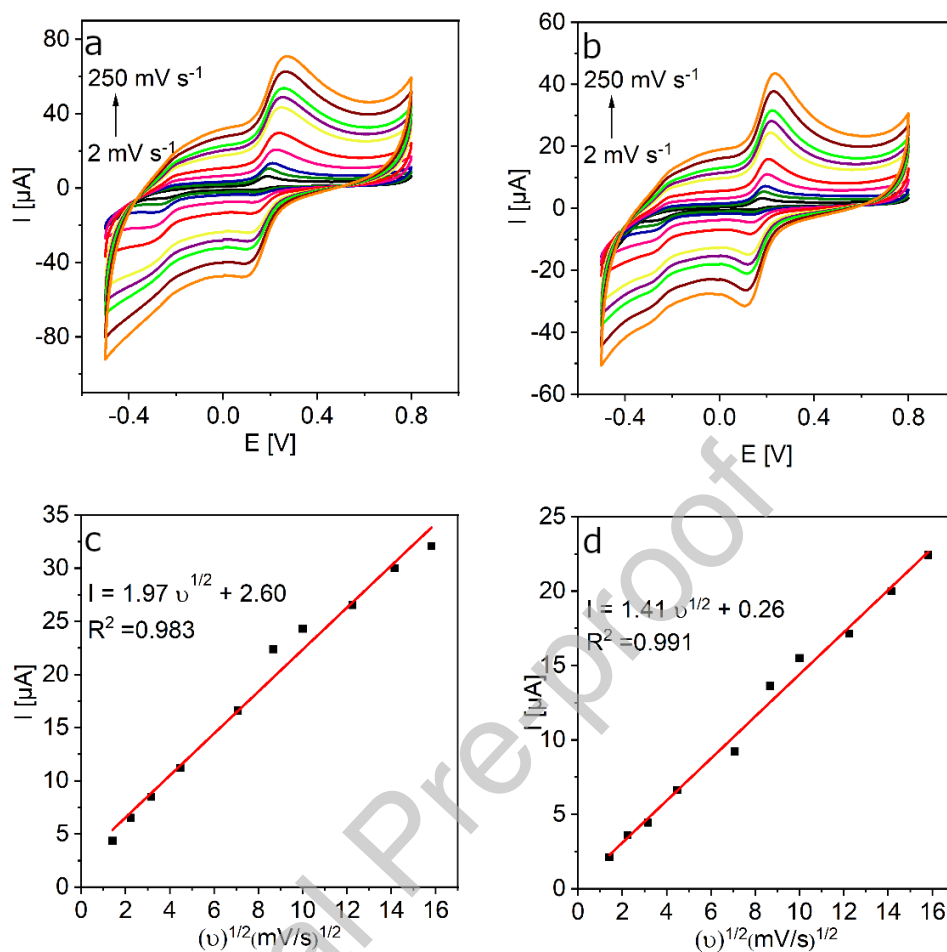


Figure 5. CVs recorded on GCEs modified with the composites (a) PANI/TRGO-400 and (b) PANI/TRGO-700 at increasing scan rates in 0.1 M PBS (pH = 7.0) containing 100 μM of DA. Relation between the DA oxidation current and square root of the v_{scan} for (c) PANI/TRGO-400 and (d) PANI/TRGO-700.

To determine the mechanism that mainly controls the kinetics of DA oxidation, the influence of the scan rate on the anodic redox process was investigated by CV in the range of 2–250 mV s^{-1} (Figure 5a and b). According to the obtained CVs, the oxidation peak potentials and currents increase for both electrodes when increasing the scan rate. However, more defined peaks and lower capacitive currents are measured with the PANI/TRGO-700 electrode. Figure 5c and d illustrate

the linear relation between the oxidation currents (Figure S5) and square root of the scan rate, thus confirming diffusion as the main mechanism influencing DA oxidation on both electrodes [44]. These results indicate the suitability of the synthesized composite materials as electrochemical platforms for DA sensing.

3.2.3. Calibration curves, LOD values, linear ranges and sensitivity of the PANI/TRGO-based sensors

To carry out the calibration of the PANI/TRGO composites for DA sensing, DPV experiments were performed, as this electrochemical technique is highly suitable for measuring faradaic currents related to redox reactions [45]. Figure 6a–b presents the baseline-corrected DPVs and the related calibration curves recorded on the GCEs modified with PANI/TRGO-400 and PANI/TRGO-700, respectively.

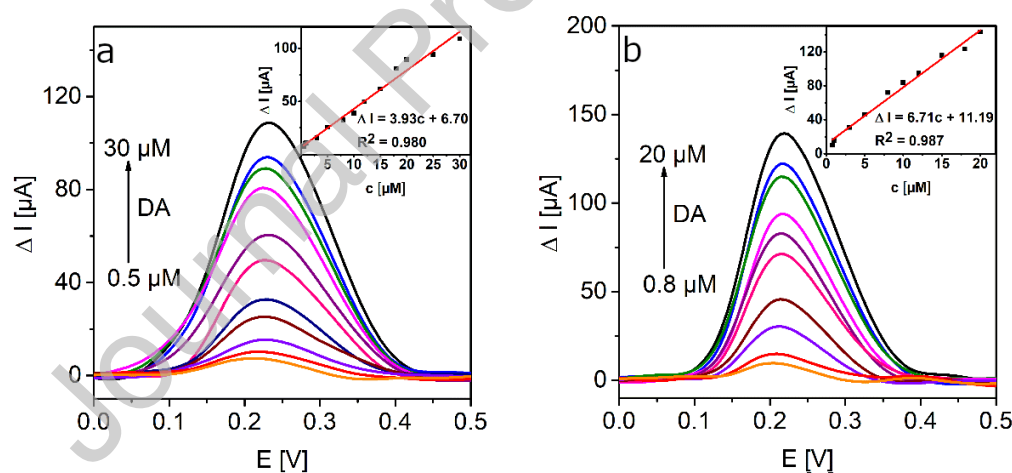


Figure 6. Baseline-corrected DPVs recorded on GCEs modified with the composites (a) PANI/TRGO-400 and (b) PANI/TRGO-700 in 0.1 M PBS solution (pH 7.0) containing increasing DA concentrations. Insets show the related calibration curves.

According to the obtained results, the anodic currents related to DA oxidation increase linearly on both electrodes with increasing concentrations of the target analyte. The correlation coefficients

(R^2) of the corresponding calibration curves are 0.980 and 0.987 for PANI/TRGO-400 and PANI/TRGO-700, respectively, corroborating the suitability of the estimated operational parameters. The LOD values for the two sensors under evaluation (signal-to-noise ratio, $S/N = 3$) were calculated according to the following equation:

$$\text{LOD} = 3S/b$$

where S is the standard deviation of the blank sample and b is the slope of the related calibration curve. Table 4 compares the LOD values, linear ranges and sensitivities calculated for the synthesized composite materials with similar previously reported active electrode materials.

Table 4. Operational parameters of the graphene materials and their binary composite-based sensors for DA sensing

Active electrode material	LOD [nM]	LR [μM]	Sensitivity [$\mu\text{A } \mu\text{M}^{-1}$]	Reference
N-rGO-180-8	630	2.5–100	2.22	[16]
PANI-GO	500	2–18	2.00	[19]
Ag-rGO	1000	10–70	0.11	[46]
N-rGO/MnO	3000	10–180	0.09	[47]
N-rGO/PEI*	500	1–130	0.06	[48]
N-rGO	930	120–220	-	[49]
PPy-rGO	1	0.01–10	6.33	[50]
PANI/TRGO-400	701	0.5–30	3.63	This work
PANI/TRGO-700	430	0.8–20	6.71	This work

*N-rGO/polyethyleneimine

The sensing parameters of the two proposed composites for DA detection are in the same range or even improved in comparison to previously reported parameters. Moreover, the PANI/TRGO composites exhibit excellent sensitivities at desirable linear ranges, maintaining low LOD values and confirming their remarkable electrochemical performance as active sensing materials. Furthermore, PANI/TRGO-700 shows better sensing parameters than PANI/TRGO-400, presenting a markedly lower LOD value (430 vs. 701 nm) and a significantly higher sensitivity (6.71 vs. 3.63 $\mu\text{A } \mu\text{M}^{-1}$). Its lower LOD is the result of its higher C_{sp^2} content and greater degree

of protonation. Both factors positively influence the electrical conductivity of the sensor. Even with a lower oxygen content, the appropriate amount and type of surface oxygen groups may be enough to facilitate the attraction of cationic DA towards the electrode/electrolyte interface, enhancing the sensitivity of the sensor. The obtained DPV results corroborate the importance of tailoring the oxygen content and electrical conductivity of the active electrode materials. This has been achieved through the fabrication of PANI/TRGO composites by hydrothermal treatment. These materials combine the suitable physicochemical properties of TRGOs, obtained at optimized temperatures, and the introduction of PANI into the graphene-based structure.

3.2.4. Selectivity of the composite-based sensors for DA detection in the presence of different interferents

The selectivity of the composite materials PANI/TRGO-400 and PANI/TRGO-700 for DA detection was evaluated by means of DPV experiments at increasing DA concentrations while maintaining fixed concentrations of AA and UA (300 μM). These commonly investigated interfering species have been selected as they both experience anodic processes at potential values close to those related to DA oxidation, thus influencing the analytical results [9]. Figure 7 presents the corresponding baseline-corrected DPVs.

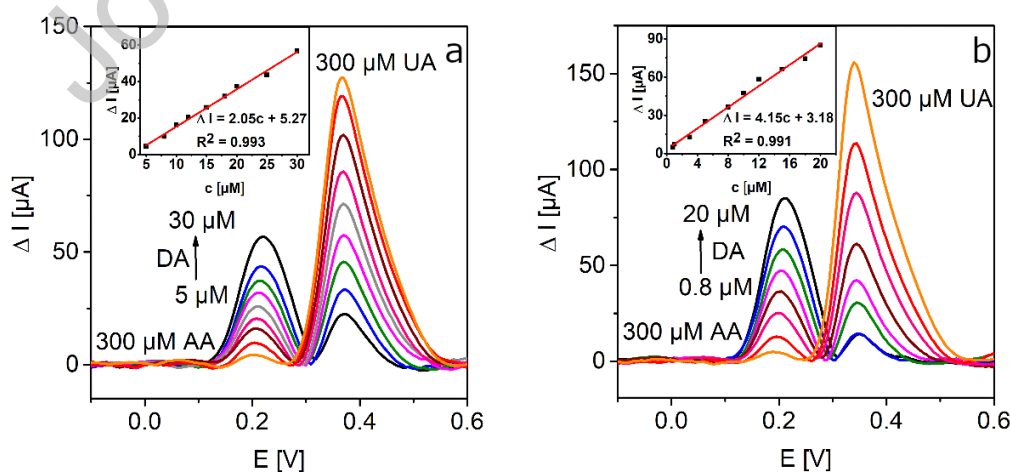


Figure 7. Baseline-corrected DPVs recorded on GCEs modified with the composites (a) PANI/TRGO-400 and (b) PANI/TRGO-700 in 0.1 M PBS solution (pH 7.0) containing increasing DA concentrations, 300 μM AA and 300 μM UA. The insets show the related calibration curves.

As shown in Figure 7, when both composites are used as active electrode materials, clearly and properly resolved anodic peaks attributed to DA oxidation (at 219 and 209 mV for PANI/TRGO-400 and PANI/TRGO-700, respectively) are developed. Furthermore, anodic peaks related to UA oxidation are observed on both electrodes (at 369 and 344 mV for PANI/TRGO-400 and PANI/TRGO-700, respectively). A decrease in the linear range, as in the case of the PANI/TRGO-400 composite, is due to attraction of the anionic UA form by the oppositely charged nitrogen groups, which mainly covers the outer surface of the graphene layers [2]. The intensity of the UA anodic peak is also higher on this electrode. In addition, no peaks related to redox processes corresponding to AA are observed on either of the two electrodes. This fact, together with the decreased signal of UA when increasing the DA concentration, can be explained by the enhanced attraction of cationic DA to the electrode/electrolyte interface due to the presence of electronegative oxygen functional groups on the surface of the active materials [16]. Even though both sensors based on PANI/TRGO can clearly distinguish the voltammetric responses of the two electrochemically active compounds, the use of PANI/TRGO-700 as active material enhances its electrochemical performance for DA detection. The LOD value calculated for the solution containing DA, UA and AA is significantly lower on the PANI/TRGO-700 electrode than that on the PANI/TRGO-400 electrode (672 vs. 1150 nM). Furthermore, the sensitivity of PANI/TRGO-700 decreases to 62% of its initial value (4.15 vs. 6.71 $\mu\text{A } \mu\text{M}^{-1}$), while PANI/TRGO-400 exhibits a decrease of 56% of its initial value (2.05 vs. 3.63 $\mu\text{A } \mu\text{M}^{-1}$). These results strengthen the suitability of PANI/TRGO-700 as an active electrode material for DA detection in the presence of

AA and UA due to its appropriate combination of surface chemistry and electrical conductivity. In addition, to further investigate the impact of other substances coexisting in the urine on DA detection, glucose (100 μM), NaCl (1100 μM), KCl (600 μM) and creatinine (80 μM), were also investigated as interfering species (Figure S6, Supporting Information). The concentrations of these interferents were selected according to their real concentrations in the human urine. After carrying out the corresponding DPV measurements, the electrochemical performance of the sensors under evaluation resulted comparable in terms of linear ranges to that showed without any interferences. The LOD values for DA detection were 933 and 459 nM for PANI/TRGO-400 and PANI/TRGO-700, respectively. Moreover, both composites-based sensors maintained 62 and 83% of their sensitivity, respectively. The absence of peaks related to the evaluated interfering substances confirms the very promising suitability of the sensors developed for real sample analysis.

3.2.5 Reproducibility, repeatability and stability of the PANI/TRGO-based sensors for DA detection

The reproducibility of the composite-based sensors was evaluated on five different electrodes. The relative standard deviation (RSD) of the DA anodic signal is 6.6 and 4.0% for PANI/TRGO-400 and PANI/TRGO-700. The repeatability is determined by measuring the anodic signal of five independent solutions containing 100 μM DA. The RSD is 5.5 and 1.0% for PANI/TRGO-400 and PANI/TRGO-700. The stability is determined by measuring the DA oxidation peak every day and then performing control measurements after 30 days (Figure 8). After 7 days, the DA oxidation signal decreases to 78.3 and 80.4% on PANI/TRGO-400 and PANI/TRGO-700, respectively. After 30 days, the response maintains almost the same value that was recorded on the 7th day (84.1

and 82.5% for PANI/TRGO-400 and PANI/TRGO-700). The obtained results demonstrate a remarkable PANI/TRGO-based sensor performance, showing the significantly better electrochemical behavior of PANI/TRGO-700 as a GCE modifier, and confirming the positive influence of its physicochemical properties on the sensor performance for DA detection.

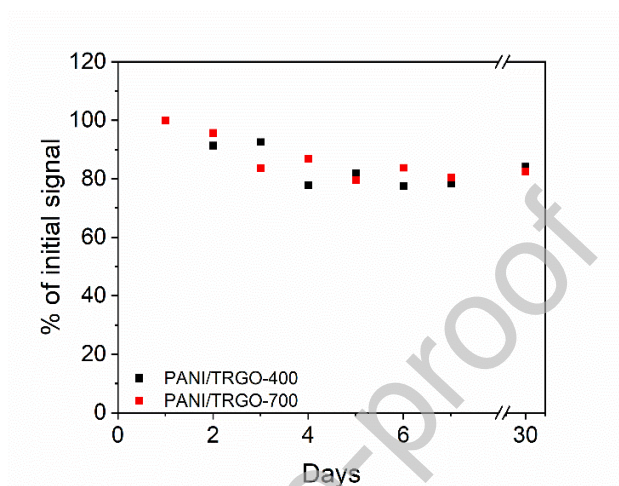


Figure 8. Long-term stability of the PANI/TRGO composites in 100 μM DA (PBS 7.0).

4. Conclusions

In this paper, the performance of PANI/TRGO composites as active electrode materials for DA detection was shown. The significant impact of the degree of reduction of the starting TRGO was revealed. A more homogenous distribution of PANI was achieved for the composite obtained with TRGO-700, which was attributed to its higher exfoliation degree compared to TRGO-400. Furthermore, using thermal reduction as the first step of the synthesis process enabled tailoring the oxygen content in the final composite, which was key for maintaining an appropriate balance between the electrical conductivity and the affinity of the cationic DA to the electrode/electrolyte interface. Due to its suitable properties, the use of PANI/TRGO-700 as active electrode material allowed to achieve a low dopamine LOD value (430 nM), in a linear range between 0.8 - 20 μM , and an outstanding sensitivity ($6.71 \mu\text{A} \mu\text{M}^{-1}$). Moreover, linking the graphene material and PANI

had a positive influence on the long-term stability of the electrochemical performance of the composite, maintaining 80% of the initial oxidation signal after 30 days. The excellent performance of the PANI/TRGO-based GCE for dopamine detection encourages the development of new TRGO-containing active materials for the detection of different analytes.

ACKNOWLEDGEMENT

Following research was financially supported by a statutory activity subsidy from the Polish Ministry of Education and Science for the Faculty of Chemistry of Wrocław University of Science and Technology.

APPENDIX

(Figure S1) XRD patterns of PANI/TRGO-400 and PANI/TRGO-700; (Figure S2) Deconvolution of the (a) N1s and (b,c,d) C1s core-level XPS spectra of the starting materials; (Figure S3) Baseline-corrected DA oxidation peaks recorded by CV on the bare and modified GCE electrodes in 0.1 M PBS (pH 7.0) containing 100 μM of DA at a scan rate of 100 mV s^{-1} ; (Figure S4) Baseline-corrected DA oxidation peaks recorded by CV on the GCEs modified with composite materials in 0.1 M PBS at increasing pH values containing 100 μM of DA at a scan rate of 100 mV s^{-1} ; (Figure S5) Baseline-corrected DA oxidation peaks recorded by CV on the composites-modified GCE in 0.1 M PBS (at optimal pH 7.0) containing 100 μM of DA at increasing scan rate (ranging from 2 to 250 mV s^{-1}); (Figure S6) Baseline-corrected DPVs recorded on GCEs modified with the composites (a) PANI/TRGO-400 and (b) PANI/TRGO-700 in 0.1 M PBS solution (pH 7.0) containing increasing DA concentrations, 800 μM creatinine, 1000 μM glucose, 600 μM KCl and 1100 μM NaCl. The insets show the related calibration curves.

Authorship contributions

Category 1

Conception and design of study: *Daria Minta, Zoraida González, Sonia Melendi-Espina, Grażyna Gryglewicz*

acquisition of data: *Daria Minta*

analysis and/or interpretation of data: *Daria Minta, Zoraida González, Sonia Melendi-Espina, Grażyna Gryglewicz*

Category 2

Drafting the manuscript: *Daria Minta, Zoraida González, Sonia Melendi-Espina, Grażyna Gryglewicz*

revising the manuscript critically for important intellectual content: *Daria Minta, Zoraida González, Sonia Melendi-Espina, Grażyna Gryglewicz*

Category 3

Approval of the version of the manuscript to be published (the names of all authors must be listed): *Daria Minta, Zoraida González, Sonia Melendi-Espina, Grażyna Gryglewicz*

Declaration of interests

The authors declare that they have no known competing financial interests or personal relationships that could have appeared to influence the work reported in this paper.

REFERENCES

- [1] R. Santhosh Kumar, K. Govindan, S. Ramakrishnan, A.R. Kim, J.S. Kim, D.J. Yoo, Fe₃O₄ nanorods decorated on polypyrrole/reduced graphene oxide for electrochemical detection of dopamine and photocatalytic degradation of acetaminophen, *Appl. Surf. Sci.* 556 (2021) pp. 149765.
- [2] J. Feng, Q. Li, J. Cai, T. Yang, J. Chen, X. Hou, Electrochemical detection mechanism of

dopamine and uric acid on titanium nitride-reduced graphene oxide composite with and without ascorbic acid, *Sensors Actuators, B Chem.* 298 (2019) pp. 126872.

- [3] F. Bashar, K. Eddin, Recent Advances in Electrochemical and Optical Sensing of Dopamine, *Sensors.* 4 (2020) pp. 1–47.
- [4] D. Butler, D. Moore, N.R. Glavin, J.A. Robinson, A. Ebrahimi, Facile Post-deposition Annealing of Graphene Ink Enables Ultrasensitive Electrochemical Detection of Dopamine, *ACS Appl. Mater. Interfaces.* 13 (2021) pp. 11185–11194.
- [5] P.M. Nowak, Simultaneous quantification of food colorants and preservatives in sports drinks by the high performance liquid chromatography and capillary electrophoresis methods evaluated using the red-green-blue model, *J. Chromatogr. A.* 1620 (2020) pp. 460976.
- [6] D. Sánchez-Rodas, W.T. Corns, B. Chen, P.B. Stockwell, Atomic Fluorescence Spectrometry: A suitable detection technique in speciation studies for arsenic, selenium, antimony and mercury, *J. Anal. At. Spectrom.* 25 (2010) pp. 933–946.
- [7] G. Han, J. Cai, C. Liu, J. Ren, X. Wang, J. Yang, X. Wang, Highly sensitive electrochemical sensor based on xylan-based Ag@CQDs-rGO nanocomposite for dopamine detection, *Appl. Surf. Sci.* 541 (2021) pp. 148566.
- [8] N. Hareesha, J.G. Manjunatha, Fast and enhanced electrochemical sensing of dopamine at cost-effective poly(DL-phenylalanine) based graphite electrode, *J. Electroanal. Chem.* 878 (2020) pp. 114533.
- [9] M.L. Huffman, B.J. Venton, Electrochemical properties of different carbon-fiber

- microelectrodes using fast-scan cyclic voltammetry, *Electroanalysis*. 20 (2008) pp. 2422–2428.
- [10] M. Sajid, M.K. Nazal, M. Mansha, A. Alsharaa, S.M.S. Jillani, C. Basheer, Chemically modified electrodes for electrochemical detection of dopamine in the presence of uric acid and ascorbic acid: A review, *TrAC - Trends Anal. Chem.* 76 (2016) pp. 15–29.
- [11] A. Pandikumar, G.T. Soon How, T.P. See, F.S. Omar, S. Jayabal, K.Z. Kamali, N. Yusoff, A. Jamil, R. Ramaraj, S.A. John, H.N. Lim, N.M. Huang, Graphene and its nanocomposite material based electrochemical sensor platform for dopamine, *RSC Adv.* 4 (2014) pp. 63296–63323.
- [12] J.M. Moon, N. Thapliyal, K.K. Hussain, R.N. Goyal, Y.B. Shim, Conducting polymer-based electrochemical biosensors for neurotransmitters: A review, *Biosens. Bioelectron.* 102 (2018) pp. 540–552.
- [13] J. Scotto, E. Piccinini, C. von Bilderling, L.L. Coria-Oriundo, F. Battaglini, W. Knoll, W.A. Marmisolle, O. Azzaroni, Flexible conducting platforms based on PEDOT and graphite nanosheets for electrochemical biosensing applications, *Appl. Surf. Sci.* 525 (2020) pp. 146440.
- [14] K.S. Novoselov, V.I. Fal'Ko, L. Colombo, P.R. Gellert, M.G. Schwab, K. Kim, A roadmap for graphene, *Nature*. 490 (2012) pp. 192-200.
- [15] M.R. Rezapour, C.W. Myung, J. Yun, A. Ghassami, N. Li, S.U. Yu, A. Hajibabaei, Y. Park, K.S. Kim, Graphene and Graphene Analogs toward Optical, Electronic, Spintronic, Green-Chemical, Energy-Material, Sensing, and Medical Applications, *ACS Appl. Mater.*

Interfaces. 9 (2017) pp. 24393–24406.

- [16] P. Wiench, Z. González, R. Menéndez, B. Grzyb, G. Gryglewicz, Beneficial impact of oxygen on the electrochemical performance of dopamine sensors based on N-doped reduced graphene oxides, *Sensors Actuators, B Chem.* 257 (2018) pp. 143–153.
- [17] P. Álvarez, C. Blanco, R. Santamaría, P. Blanco, Z. González, L. Fernández-García, U. Sierra, M. Granda, A. Páez, R. Menéndez, Tuning graphene properties by a multi-step thermal reduction process, *Carbon N. Y.* 90 (2015) pp. 160–163.
- [18] I. Sengupta, S. Chakraborty, M. Talukdar, Thermal reduction of graphene oxide : How temperature influences purity, *J. Mater. Research.* 33 (2018) pp. 4113-4122.
- [19] P. Manivel, M. Dhakshnamoorthy, A. Balamurugan, N. Ponpandian, D. Mangalaraj, C. Viswanathan, Conducting polyaniline-graphene oxide fibrous nanocomposites: Preparation, characterization and simultaneous electrochemical detection of ascorbic acid, dopamine and uric acid, *RSC Adv.* 3 (2013) pp. 14428–14437.
- [20] D. Minta, A. Moyseowicz, S. Gryglewicz, G. Gryglewicz, A Promising Electrochemical Platform for Dopamine and Uric Acid Detection Based on a Polyaniline/Iron Oxide-Tin Oxide/Reduced Graphene Oxide Ternary Composite, *Molecules.* (2020) pp. 5869.
- [21] O.E. Fayemi, A.S. Adekunle, B.E. Kumara Swamy, E.E. Ebenso, Electrochemical sensor for the detection of dopamine in real samples using polyaniline/NiO, ZnO, and Fe₃O₄ nanocomposites on glassy carbon electrode, *J. Electroanal. Chem.* 818 (2018) pp. 236–249.
- [22] T.K. Aparna, R. Sivasubramanian, M.A. Dar, One-pot synthesis of Au-Cu₂O/rGO nanocomposite based electrochemical sensor for selective and simultaneous detection of

- dopamine and uric acid, *J. Alloys Compd.* 741 (2018) pp. 1130–1141.
- [23] D. Minta, Z. González, P. Wiench, S. Gryglewicz, G. Gryglewicz, N-doped reduced graphene oxide/gold nanoparticles composite as an improved sensing platform for simultaneous detection of dopamine, ascorbic acid, and uric acid, *Sensors (Switzerland)*. 20 (2020) pp. 1–13.
- [24] L. Yang, D. Liu, J. Huang, T. You, Simultaneous determination of dopamine, ascorbic acid and uric acid at electrochemically reduced graphene oxide modified electrode, *Sensors Actuators, B Chem.* 193 (2014) pp. 166–172.
- [25] F. Gao, X. Cai, X. Wang, C. Gao, S. Liu, F. Gao, Q. Wang, Highly sensitive and selective detection of dopamine in the presence of ascorbic acid at graphene oxide modified electrode, *Sensors Actuators, B Chem.* 186 (2013) pp. 380–387.
- [26] Y.R. Kim, S. Bong, Y.J. Kang, Y. Yang, R.K. Mahajan, J.S. Kim, H. Kim, Electrochemical detection of dopamine in the presence of ascorbic acid using graphene modified electrodes, *Biosens. Bioelectron.* 25 (2010) pp. 2366-9.
- [27] E. Jin, X. Lu, X. Bian, L. Kong, W. Zhang, C. Wang, Unique tetragonal starlike polyaniline microstructure and its application in electrochemical biosensing, *J. Mater. Chem.* 15 (2010) pp. 3079–3083.
- [28] L. Yang, S. Liu, Q. Zhang, F. Li, Simultaneous electrochemical determination of dopamine and ascorbic acid using AuNPs@polyaniline core-shell nanocomposites modified electrode, *Talanta.* 89 (2012) pp. 136–141.
- [29] W.S. Hummers, R.E. Offeman, Preparation of Graphitic Oxide, *J. Am. Chem. Soc.* 80

(1958) pp. 1339.

- [30] A. Moyseowicz, G. Gryglewicz, Hydrothermal-assisted synthesis of a porous polyaniline/reduced graphene oxide composite as a high-performance electrode material for supercapacitors, *Compos. Part B Eng.* 159 (2019) pp. 4–12.
- [31] L.B. Valdes, Resistivity Measurements on Germanium for Transistors, *Proc. IRE.* 42 (1954) pp. 420–427.
- [32] F.M. Smits, Measurement of Sheet Resistivities with the Four-Point Probe, *Bell Syst. Tech. J.* 37 (1958) pp. 711–718.
- [33] W. Lyu, M. Yu, J. Feng, W. Yan, Facile synthesis of coral-like hierarchical polyaniline micro/nanostructures with enhanced supercapacitance and adsorption performance, *Polymer (Guildf).* 162 (2019) pp. 130–138.
- [34] C. Botas, P. Álvarez, C. Blanco, R. Santamaría, M. Granda, M.D. Gutiérrez, F. Rodríguez-Reinoso, R. Menéndez, Critical temperatures in the synthesis of graphene-like materials by thermal exfoliation-reduction of graphite oxide, *Carbon N. Y.* 52 (2013) pp. 476–485.
- [35] A. Celzard, J.F. Marêché, G. Furdin, Surface area of compressed expanded graphite, *Carbon N. Y.* 40 (2002) pp. 2713–2718.
- [36] A. Moyseowicz, A. Śliwak, E. Miniach, G. Gryglewicz, Polypyrrole/iron oxide/reduced graphene oxide ternary composite as a binderless electrode material with high cyclic stability for supercapacitors, *Compos. Part B Eng.* 109 (2017) pp. 23–29.
- [37] B. Gupta, N. Kumar, K. Panda, V. Kanan, S. Joshi, I. Visoly-Fisher, Role of oxygen functional groups in reduced graphene oxide for lubrication, *Sci. Rep.* 7 (2017) pp. 1–14.

- [38] E.A. Sanches, J.C. Soares, R.M. Iost, V.S. Marangoni, G. Trovati, T. Batista, A.C. Mafud, V. Zucolotto, Y.P. Mascarenhas, Structural characterization of emeraldine-salt polyaniline/gold nanoparticles complexes, *J. Nanomater.* 2011 (2011) pp. 1–8.
- [39] A. Moysowicz, Z. González, R. Menéndez, G. Gryglewicz, Three-dimensional poly(aniline-co-pyrrole)/thermally reduced graphene oxide composite as a binder-free electrode for high-performance supercapacitors, *Compos. Part B Eng.* 145 (2018) pp. 232–239.
- [40] S. Golczak, A. Kancierzewska, M. Fahlman, K. Langer, J.J. Langer, Comparative XPS surface study of polyaniline thin films, *Solid State Ionics.* 179 (2008) pp. 2234–2239.
- [41] C.S. Martin, C. Gouveia-Caridade, F.N. Crespilho, C.J.L. Constantino, C.M.A. Brett, Iron Phthalocyanine Electrodeposited Films: Characterization and Influence on Dopamine Oxidation, *J. Phys. Chem. C.* 120 (2016) pp. 15698–15706.
- [42] E. Casero, A.M. Parra-Alfambra, M.D. Petit-Domínguez, F. Pariente, E. Lorenzo, C. Alonso, Differentiation between graphene oxide and reduced graphene by electrochemical impedance spectroscopy (EIS), *Electrochem. Commun.* 20 (2012) pp. 63–66.
- [43] N. Baig, A.-N. Kawde, M. Ibrahim, Efficient ionic medium supported reduced graphene oxide-based sensor for selective sensing of dopamine, *Mater. Adv.* 1 (2020) pp. 783–793.
- [44] S. Sundar, G. Venkatachalam, S.J. Kwon, Biosynthesis of copper oxide (CuO) nanowires and their use for the electrochemical sensing of dopamine, *Nanomaterials.* 8 (2018) pp. 823.
- [45] P.S. Dorraji, F. Jalali, Novel sensitive electrochemical sensor for simultaneous determination of epinephrine and uric acid by using a nanocomposite of MWCNTs-chitosan

and gold nanoparticles attached to thioglycolic acid, *Sensors Actuators, B Chem.* 200 (2014) pp. 251–258.

- [46] S.P. Nayak, S.S. Ramamurthy, J.K. Kiran Kumar, Green synthesis of silver nanoparticles decorated reduced graphene oxide nanocomposite as an electrocatalytic platform for the simultaneous detection of dopamine and uric acid, *Mater. Chem. Phys.* 252 (2020) pp. 123302.
- [47] R. Chen, Y. Wang, Y. Liu, J. Li, Selective electrochemical detection of dopamine using nitrogen-doped graphene/manganese monoxide composites, *RSC Adv.* 5 (2015) pp. 85065–85072.
- [48] N. Li, E. Zheng, X. Chen, S. Sun, Y. Ruan, X. Weng, C. You, Layer-by-layer assembled multilayer films of nitrogen-doped graphene and polyethylenimine for selective sensing of dopamine, *Int. J. Electrochem. Sci.* 8 (2013) pp. 6524–6534.
- [49] S.M. Li, S.Y. Yang, Y.S. Wang, C.H. Lien, H.W. Tien, S.T. Hsiao, W.H. Liao, H.P. Tsai, C.L. Chang, C.C.M. Ma, C.C. Hu, Controllable synthesis of nitrogen-doped graphene and its effect on the simultaneous electrochemical determination of ascorbic acid, dopamine, and uric acid, *Carbon N. Y.* 59 (2013) pp. 418–429.
- [50] T. Qian, S. Wu, J. Shen, Facilely prepared polypyrrole-reduced graphite oxide core-shell microspheres with high dispersibility for electrochemical detection of dopamine, *Chem. Commun.* 49 (2013) pp. 4610–4612.

Table of content

Figure 1. SEM images of (a) PANI, (b) TRGO-400, (c) TRGO-700, (d) PANI/TRGO-400 and (e) PANI/TRGO-700.

Figure 2. Deconvolution of the (a, b) C1s core-level XPS spectra of PANI/TRGO-400 and PANI/TRGO-700, respectively, and (c, d) N1s core-level XPS spectra of PANI/TRGO-400 and PANI/TRGO-700, respectively.

Figure 3. CVs recorded on the bare and modified GCEs in a 0.1 M PBS (pH 7.0) solution containing 100.0 μM DA at a scan rate of 100 mVs^{-1} (a). Nyquist plots recorded on the bare and modified GCEs in PBS (pH=7.0) solution containing 10 mM $[\text{Fe}(\text{CN})_6]^{3-/4-}$ at a formal potential of 0.27 V and a frequency range of 0.1–10⁵ kHz (b). The inset shows an expanded view of the high-frequency region of the Nyquist plots. The selected equivalent circuit is shown below the plots to fit the impedance data.

Figure 4. CVs recorded ($v_{\text{scan}} = 100 \text{ mVs}^{-1}$) at increasing pH values on GCEs modified with the composites (a) PANI/TRGO-400 and (b) PANI/TRGO-700 in 0.1 M PBS solution containing 100 μM of DA. Influence of the selected pH on the oxidation current and peak potential values on GCEs modified with (c) PANI/TRGO-400 and (d) PANI/TRGO-700.

Figure 5. CVs recorded on GCEs modified with the composites (a) PANI/TRGO-400 and (b) PANI/TRGO-700 at increasing scan rates in 0.1 M PBS (pH = 7.0) containing 100 μM of DA. Relation between the DA oxidation current and square root of the v_{scan} for (c) PANI/TRGO-400 and (d) PANI/TRGO-700.

Figure 6. Baseline-corrected DPVs recorded on GCEs modified with the composites (a) PANI/TRGO-400 and (b) PANI/TRGO-700 in 0.1 M PBS solution (pH 7.0) containing increasing DA concentrations. Insets show the related calibration curves.

Figure 7. Baseline-corrected DPVs recorded on GCEs modified with the composites (a) PANI/TRGO-400 and (b) PANI/TRGO-700 in 0.1 M PBS solution (pH 7.0) containing increasing DA concentrations, 300 μ M AA and 300 μ M UA. The insets show the related calibration curves.

Figure 8. Long-term stability of the PANI/TRGO composites in 100 μ M DA (PBS 7.0).

Table 1. Characteristics of the starting and composite materials.

Table 2. Results of C1s and N1s spectra deconvolution (at. %)

Table 3. Impedance data measured for the bare and modified GCE electrodes

Table 4. Operational parameters of the graphene materials and their binary composite-based sensors for DA sensing